Direct chemical evidence for eumelanin pigment from the Jurassic period

Keely Glass[a], Shosuke Ito[b,1], Philip R. Wilby[c,1], Takayuki Sota[d], Atsushi Nakamura[d], C. Russell Bowers[e], Jakob Vinther[f], Suryendu Dutta[g,h], Roger Summons[g], Derek E. G. Briggs[f], Kazumasa Wakamatsu[b], and John D. Simon[a,i,1]

[a]Department of Chemistry, Duke University, Durham, NC 27708; [b]Department of Chemistry, Fujita Health University School of Health Sciences, Toyoake, Aichi 470-1192, Japan; [c]British Geological Survey, Keyworth, Nottingham NG12 5GG, United Kingdom; [d]Department of Electrical Engineering and Bioscience, Waseda University, Tokyo 169-8555, Japan; [e]Department of Chemistry, University of Florida, Gainesville, FL 32611; [f]Department of Geology and Geophysics, Yale University, New Haven, CT 06520; [g]Department of Earth, Atmospheric and Planetary Sciences, Massachusetts Institute of Technology, Cambridge, MA 02139; [h]Department of Earth Sciences, Indian Institute of Technology Bombay, Powai, Mumbai-400076, India; and [i]Department of Chemistry, University of Virginia, Charlottesville, VA 22904.

Edited by Luigi Zecca, Italian National Research Council, Segrate, Italy, and accepted by the Editorial Board April 2, 2012 (received for review November 9, 2011)

Melanin is a ubiquitous biological pigment found in bacteria, fungi, plants, and animals. It has a diverse range of ecological and biochemical functions, including display, evasion, photoprotection, detoxification, and metal scavenging. To date, evidence of melanin in fossil organisms has relied entirely on indirect morphological and chemical analyses. Here, we apply direct chemical techniques to categorically demonstrate the preservation of eumelanin in two >160 Ma Jurassic cephalopod ink sacs and to confirm its chemical similarity to the ink of the modern cephalopod, *Sepia officinalis*. Identification and characterization of degradation-resistant melanin may provide insights into its diverse roles in ancient organisms.

Exceptional preservation of soft tissue is rare in the fossil record because microbial decomposition is highly efficient (1, 2). Tissues that do survive are subject to diagenetic alteration whereby their organic constituents polymerize into long chains of hydrocarbons that are resistant to further degradation (2). Little original organic chemistry or ultrastructure is typically retained in fossils more than 65 Ma (2). Biomolecules that are polymeric and highly cross-linked in their original state exhibit the greatest resistance to alteration (1, 2). Melanin, a complex biopolymer, meets this high-resistance criterion. Two forms of melanin, produced from different molecular precursors, are present in nature—eumelanin (dark brown-black in color) and pheomelanin (orange-red in color) (3). These classes of melanin serve numerous essential biological roles, including photoprotection, radioprotection, display, camouflage, and predation avoidance (4, 5).

Recent reports have relied on indirect methods to confirm the presence and distribution of melanin in the fossil record (6, 7). Chelate metal traces have been used as a proxy for determining the density and distribution of eumelanin in a wide range of taxa, and plumage patterns in dinosaurs have been reconstructed using visual evidence of organelle-like structures containing melanin pigment (8–10).

The Peterborough Member of the Oxford Clay Formation (Middle Jurassic, 162 Ma) at Christian Malford, Wiltshire (UK) and the Blue Lias Formation (Lower Jurassic, 195 Ma) at Lyme Regis, Dorset (UK) yield coleoid cephalopods containing large, black ink sacs preserved in three dimensions (11). Scanning electron microscopy (SEM) images of a specimen from each of these deposits, GSM 122841 and GSM 120386 (Fig. 1 *A* and *B*), reveal that the ink is composed of globular granules similar in size and shape to that of the modern coleoid *S. officinalis* (12) (Fig. 1 *C–E*). The presence of such structures alone is insufficient to prove that melanin pigment is preserved because many microbes and minerals adopt a similar morphology (1, 13).

Fortunately, melanin has a wide range of unique chemical signatures that can be used to identify and characterize its different forms in nature (14). Here we adapt these chemical approaches to verify melanin in GSM 122841 and GSM 120386 and to compare the preserved pigment composition with that of melanin from the modern cephalopod *S. officinalis*. These fossils exceed the age beyond which significant diagenetic alteration of organic compounds normally occurs, and therefore provide a test for the wider viability of melanin biomarkers in the fossil record (15).

Results and Discussion

The single unique assay commonly used to identify modern melanins is alkaline hydrogen peroxide oxidation. Under the oxidation conditions described by Ito and collaborators, melanin breaks down into distinct chemical markers associated with its monomeric precursors (16, 17). A second fundamental method and the most used signature for melanin in physical chemistry, electron paramagnetic resonance spectroscopy (EPR), can verify the results of alkaline hydrogen peroxide oxidation. EPR probes the electronic properties of a material nondestructively (18, 19).

Alkaline hydrogen peroxide degradation was developed with an understanding of how melanin is naturally synthesized and was refined to identify eumelanin through the presence of specific chemical markers—5,6-dihydroxyindole (DHI) and 5,6-dihydroxyindole-2-carboxylic acid (DHICA) (20, 21). Eumelanin is generated from these chemical building blocks, which are derived from the amino acid tyrosine (22). The biologically controlled copolymerization of DHI and DHICA produce eumelanin pigment with an unknown absolute structure (14, 23). Alkaline hydrogen peroxide degradation breaks this copolymer into unique markers (Fig. 2*A*), pyrrole-2,3,5-tricarboxylic acid (PTCA), pyrrole-2,3-dicarboxylic acid (PDCA), pyrrole-2,3,4-tricarboxylic acid (iso-PTCA), and pyrrole-2,3,4,5-tetracarboxylic acid (PTeCA) (17, 20, 21, 24). These products are common only to eumelanin and have never been produced by the alkaline hydrogen peroxide oxidation of any other biological material (17, 21). Similarly, there are unique markers for pheomelanin—thiazole-2,4,5-tricarboxylic acid (TTCA) and thiazole-4,5-dicarboxylic acid (TDCA) (16, 17). The chemical degradation of the fossil pigments produces the expected markers for eumelanin (Fig. 2*B* and Fig. S1*A*) and no evidence of the characteristic markers for pheomelanin. This is consistent with pigment from the ink of *S. officinalis*, which is pure eumelanin. The sediment adjacent to each fossil specimen was also analyzed and yielded small quantities of the degradation markers for eumelanin ranging from 0–4.7% of the eumelanin markers found in each fossil specimen (Table S1). This eumelanin

Author contributions: K.G., S.I., and J.D.S. designed research; K.G., S.I., T.S., A.N., C.R.B., S.D., and K.W. performed research; K.G., S.I., P.R.W., T.S., A.N., C.R.B., J.V., S.D., D.E.G.B., K.W., and J.D.S. contributed new reagents/analytic tools; K.G., S.I., T.S., A.N., S.D., D.E.G.B., K.W., and J.D.S. analyzed data; and K.G. wrote the paper.

The authors declare no conflict of interest.

This article is a PNAS Direct Submission. L.Z. is a guest editor invited by the Editorial Board.

[1]To whom correspondence may be addressed. E-mail: john.simon@virginia.edu, sito@fujita-hu.ac.jp, or p.wilby@bgs.ac.uk.

This article contains supporting information online at www.pnas.org/lookup/suppl/doi:10.1073/pnas.1118448109/-/DCSupplemental.

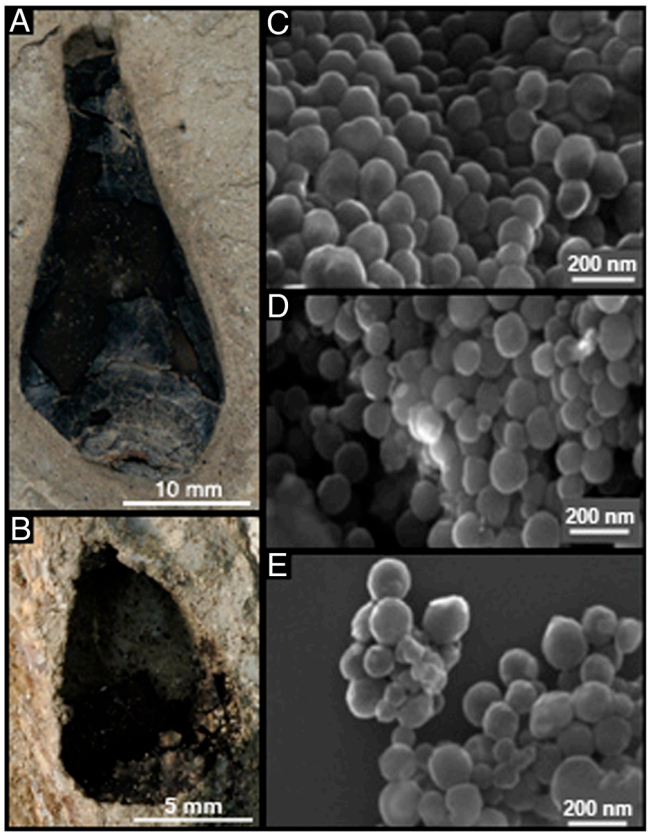

Fig. 1. Photographs of intact Jurassic coleoid ink sac specimens GSM 122841 (*A*) and GSM 120386 (*B*). SEM images of *S. officinalis* melanin (*C*), GSM 122841 (*D*), and GSM 120386 (*E*). All SEM images were taken at the same magnification. The average size of the spherical structures shown in *C*–*E* is 140 ± 20 nm, 168 ± 30 nm, and 156 ± 30 nm, respectively, where ± indicates the standard deviation.

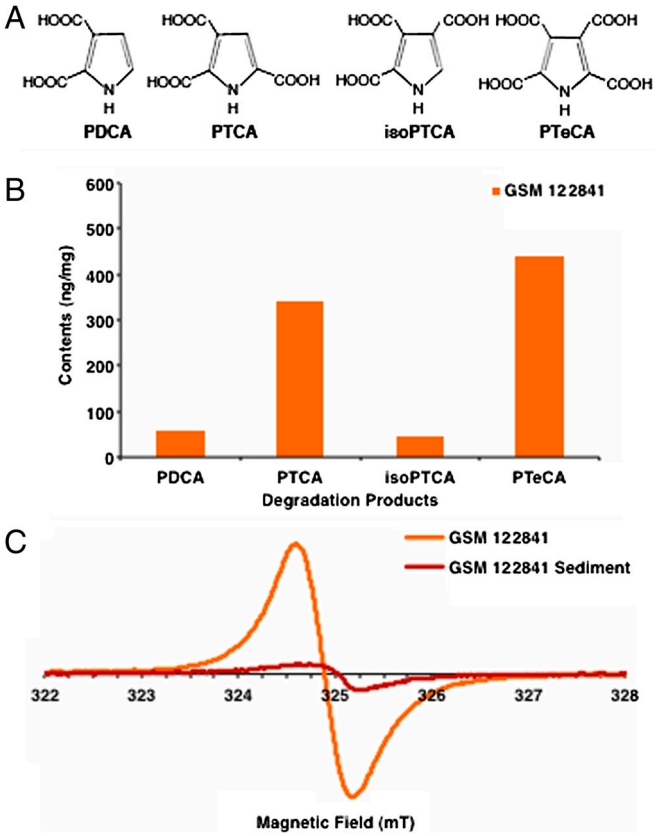

Fig. 2. (*A*) The molecular structure of the unique melanin markers. (*B*) Quantification of melanin markers produced by chemical degradation of fossil specimen GSM 122841. Degradation of the sediment of GSM 122841 yielded 1.7 ng/mg PDCA, 2.2 ng/mg PTCA, <2.2 ng/mg isoPTCA, and <1.3 ng/mg of PTeCA (Table S1). (*C*) The EPR spectra of GSM 122841 and its sediment exhibited the linewidth and g-factor characteristic of eumelanin. The same quantity of sample pigment and sediment were used to provide a qualitative comparison of the amount of eumelanin present.

in the background sediment is attributed to a small leak of pigment from the ink sacs.

The identity of each degradation marker from fossil specimen GSM 120386 was confirmed using high-resolution mass spectrometry to obtain exact mass measurements (Fig. S2 *A–D* and Table S2). The ratio of PTeCA/PTCA for both GSM 122841 and GSM 120386 is greater than that of modern *S. officinalis* (Table S1). Increase in this ratio also occurs when 1:1 DHI:DHICA synthetic eumelanin is exposed to elevated temperatures for prolonged periods, so we attribute the increased concentrations of the PTeCA marker in the fossil samples to cross linking in the eumelanin subunits as a consequence of diagenesis and thermal maturation during sedimentary burial (Table S3).

Eumelanin also possesses a unique free radical signature that originates from semiquinone species present in the pigment and can be detected by EPR (18). X-band (9.5 GHz) EPR spectra (Fig. 2*C* and Fig. S1*B*) of both fossil specimens reveal a single band with a similar linewidth and g-factor as modern *S. officinalis* eumelanin. This result also confirms the absence of pheomelanin, as the EPR signal of that pigment reveals hyperfine splitting in this frequency range. The diminished EPR signals of the background sediments also confirmed the presence of minimal eumelanin in the sediment of each specimen (Fig. 2*C* and Fig S1*B*).

In addition to the two assays discussed above, melanin solubilization in aqueous Soluene-350 is characterized by a broad, structureless absorption spectrum extending from the UV throughout the visible region (25). The absorbance at 500 nm (A_{500}) of the resulting Soluene-350 solution can be used to rapidly estimate the total amount of melanin in a sample (25). The A_{500} of the dissolved fossil specimens, background sediments, and *S. officinalis* are shown in Table S1 and further establish the presence of the pigment in the fossil specimens.

To gain further insights into the chemistry of the fossilized material, we used pyrolysis in combination with gas chromatography and mass spectroscopy (py–GC–MS), elemental analysis, fourier transform infrared spectroscopy (FTIR), and X-ray photoelectron spectroscopy (XPS). This is a powerful combination of techniques for identifying structural properties of complex organic constituents.

Py–GC–MS generates a chemical fingerprint of the degradation products produced when a sample is heated rapidly to high temperatures. The distribution of the pyrolysis products from GSM 120386 is similar to that of *S. officinalis* (Fig. S3). Major pyrolysis products are present in both the fossil and modern specimens except thiophene and its derivatives, which are absent or occur below the detection limit of pyrolysates in *S. officinalis*. The presence of thiophenes in the fossil ink and associated sediments indicates the incorporation of sulfur into the macromolecules as a consequence of bacterial sulfate reduction in the sediments (26). High-sulfur geopolymers are formed in environments lacking iron where the sulfide produced by sulfate-reducing bacteria can react preferentially with organic matter (26). It is important to note that pheomelanins produce S-containing compounds like benzothiazine and benzothiazole upon pyrolysis, but these markers were not detected in the present study (27). Fatty acids—C_{16} and C_{18}—were also produced in high abundance upon pyrolysis of extant and fossil ink samples. This lipid presence in the cephalopod ink is presumably derived from components other than

melanin itself. The high abundance of indole and methylindole, and the lack of S-containing pheomelanin markers in pyrolysates of the analyzed samples, suggest that both extant and fossilized ink samples are composed of eumelanin.

Although pyrolysis compares degradation products derived from the organic material within samples, it does not reveal the overall abundance of critical organic residues like carbon, nitrogen, oxygen, and hydrogen. Elemental analysis can provide a quantitative measure of the C, N, and H present in each sample (Table S4). GSM 120386 yielded quantities of C, N, and H close to those of DHICA-melanin, while the elemental analysis of GSM 122841 provided limited information about its chemical nature. The background sediments showed substantially lower nitrogen content than the fossil pigments (Table S4).

To gain insight into the preserved organic chemical groups in the fossil pigment, FTIR spectra were recorded. The FTIR spectrum of *S. officinalis* melanin consists of three major bands centered at 3,400 cm^{-1}, 1,605 cm^{-1}, and 1,371 cm^{-1} (28–30). The band at 3,400 cm^{-1} is dominated by absorption due to the stretching mode of the OH bond, while the band at 1,605 cm^{-1} is attributed to the carbonyl stretch in indole quinone. The band at 1,371 cm^{-1} may consist of absorption bands due to in-plane bending modes of OH and NH bonds combined with various modes of aromatic rings.

The overall FTIR spectral features of *S. officinalis* melanin are also observed in both GSM 122841 (Fig. 3*A*) and GSM 120386 (Fig. S1*C*). The fossil spectra show absorption bands derived from the CH stretching vibration in CH_x functional groups, approximately 2,856 and 2,926 cm^{-1}. The absorption bands due to these functional groups are also found in the background sediment spectra where there is no fingerprint of eumelanin. This is consistent with the presence of lipids, which are exceptionally recalcitrant, in both the fossil samples and background sediments. Second, the shoulder at 1,711 cm^{-1} becomes more apparent and distinct from the band at 1,622 cm^{-1}, suggesting that the content of indole quinone units is lower in fossil eumelanin than in modern melanin. Third, a broad absorption band at less than 1,500 cm^{-1} appears, but is accounted for by the background sediment.

The absorption bands indicated by the asterisk and stars in the background sediment FTIR spectra are due to the phosphate and carbonate groups, respectively. It is clear that hydroxyapatite, a common diagenetic mineral, is associated with these fossils, and calcium carbonate, abundant in shell material, is present in the fossil sediments (11). The carbon and hydrogen in the background sediments is due in part to the calcium carbonate and hydroxyapatite in the sediments (Table S4).

The X-ray photoelectron spectroscopy (XPS) scan, shown in Fig. 3*B*, corroborates the existence of the organic and mineral residues revealed by FTIR. XPS is not limited to identifying all of the elements present in the top 5–10 nm of a sample; it can also provide information about the binding interactions of a particular element in that sample (31). From high-resolution XPS data of the carbon peaks of GSM 122841 and GSM 120386, we determined that carbon participates in CH_x, CNH_2; C–O, C_2NH; C=O; and COO binding interactions (Fig. 4*A* and Table S5). The surface binding interactions of *S. officinalis* melanin and both fossil specimens are identical in type and relative amount. The background fossil sediment participates in many of the same surface binding interactions as the fossil pigment, but the sediment contains a carbonate and lacks a carbonyl peak (Fig. 4*C*). It is important to note that calcium carbonate only exhibits two signals, a carbonate (CO_3) signal at approximately 289.3 eV and a hydrocarbon impurity (CH_x) signal calibrated to 285 eV (32).

To verify that the organic functional groups present in the surface of the sample also pervade the bulk of the pigmented fossil, cross-polarization magic angle spinning solid-state nuclear magnetic resonance spectroscopy (CP-MAS SSNMR) was employed. The spectra of GSM122841 (Fig. 4*B*) and GSM120386 (Fig. S1*D*) confirm the presence of aliphatic groups 0–90 ppm (CH_x, CNH_2), aromatic groups 90–160 ppm (CH_x, C–O, C_2NH) and carboxylic acid groups and ketones 160–200 ppm (C=O, COO), consistent with those previously reported for *S. officinalis* (33). The spectra of the background sediments of GSM 122841 and GSM 120386 lack the aromatic, carboxylic acid, and ketone signals present in the fossil pigment (Fig. 4*D* and Fig. S1*E*). This bulk technique confirms that melanin is not present in the fossil sediments at a level detectable by CP-MAS SSNMR.

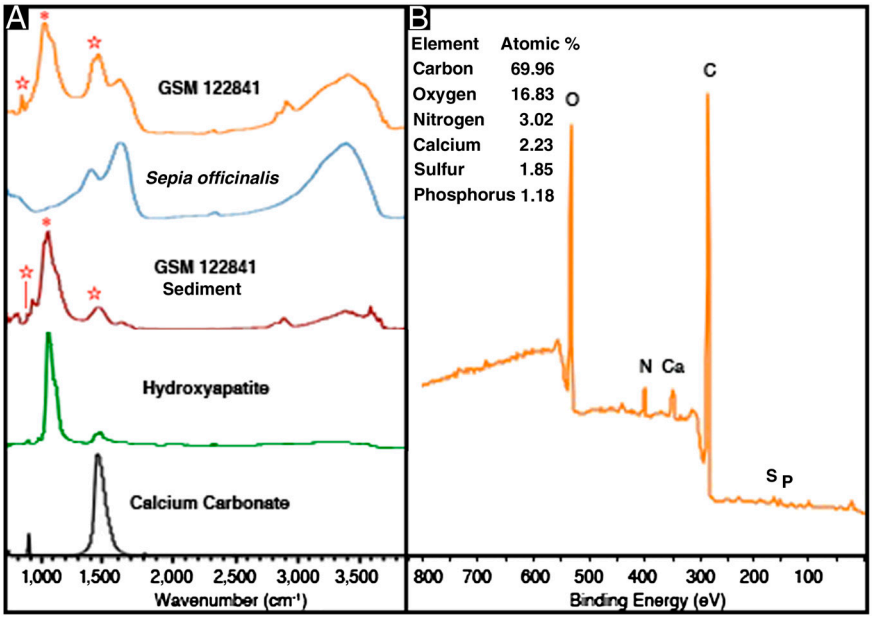

Fig. 3. (*A*) IR absorption spectra for GSM 122841, *S. officinalis* melanin, GSM 122841 sediment, and standards of hydroxyapatite and calcium carbonate. The absorption bands marked with asterisk and stars are attributed to phosphate and carbonate group, respectively. (*B*) XPS scan of GSM 122841, revealing the major elements present in the top 5–10 nm of the fossil specimen. Additional elements present in greater than 0.1 atomic % (the detection limit of the instrument) include: silicon 2.70, aluminum 2.04, and fluorine 0.18.

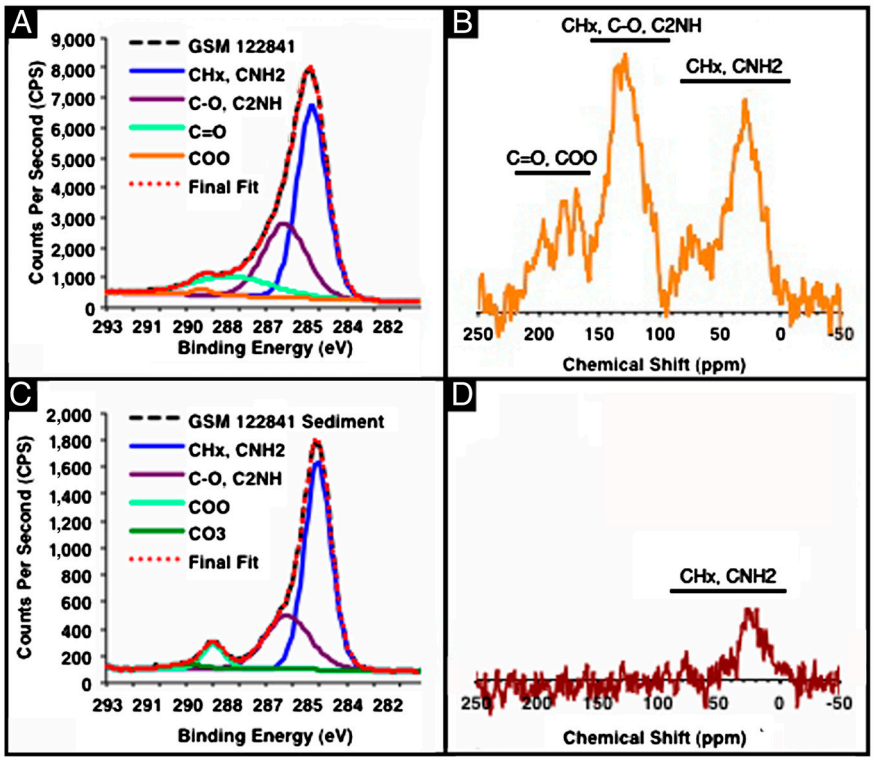

Fig. 4. (*A*) High-resolution carbon XPS scan of GSM 122841, (*B*) CP-MAS SSNMR spectrum of GSM 122841, (*C*) high-resolution carbon XPS scan of GSM 122841 sediment, and (*D*) CP-MAS SSNMR spectrum of GSM 122841 sediment. (*A*) The average percent and standard deviation of the functional groups present in the top 5–10 nm of GSM 122841 sample are, as follows: 54 ± 1, 32 ± 3, 13 ± 4, and $1 \pm 1\%$ for CH_x, CNH_2; C—O, C_2NH; C═O; and COO based on fitting with mixed Gaussian (30%) Lorentzian peaks. (*B*) The presence of the functional groups revealed in the XPS data is confirmed for the bulk sample through its SSNMR spectrum. (*C*) The average percent and standard deviation of the functional groups present in the top 5–10 nm of GSM 122841 sediment are: 65 ± 3, 26 ± 2, 6 ± 1, and $3 \pm 1\%$ for CH_x, CNH_2; C—O, C_2NH; COO; and CO_3 based on fitting with mixed Gaussian (30%) Lorentzian peaks. No C═O peak was present in the GSM 122841 sediment. (*D*) The result of the XPS analysis of the GSM 122841 sediment is corroborated by the lack of key melanin aromatic and carbonyl signals in its SSNMR spectrum.

Our results demonstrate that eumelanin persists in the fossil record for at least 160 million years, the oldest determination to date. Strikingly, within the limits of the techniques used, the preserved pigment exhibits properties that are chemically similar to modern phylogenetically related *S. officinalis*. The methods discussed here can serve to recognize and understand the distribution of melanin in ancient organisms and expand, beyond melanin, into a greater appreciation for the organic moieties hidden in the fossil record.

Materials and Methods

Fossil Specimens. GSM 122841 (Fig. 1*A*), approximately 162 million years old, was collected from the Peterborough Member of the Oxford Clay Formation (middle Jurassic, Upper Callovian) at Christian Malford, Wiltshire (UK). The Peterborough Member is dominated by fossiliferous organic-rich mudstones (34). The total organic carbon (TOC) content of the host sediment, shown in Table S6, is 11.9% and dominated by Type II (marine) and Type III (terrestrial) organic matter (35). The Rock-Eval T_{max} of the sediments is 411 °C, which indicates that the organic matter has had a very mild thermal history (Table S6). Based on molecular analysis of the organic matter, Hudson and Martill suggest that peak burial temperature may never have exceeded 40 °C in this area (36). Penn et al. suggest that maximum burial in this area was only 200–300 m (37).

GSM120386 (Fig. 1*B*), approximately 195 million years old, was collected from Bed 32 of the Blue Lias Formation (early Jurassic, Lower Sinemurian) at Lyme Regis, Dorset (UK) (38). The Blue Lias Formation consists of decimeter-scale cyclical alternations of fossiliferous mudstone and tabular or nodular argillaceous limestones (38). Lyme Regis is located within the Wessex Basin, a Mesozoic fault-bounded depocenter. The TOC content of the sediments, shown in Table S6, is 4.5%, mostly distributed between Type II (marine) and Type IV (altered) organic material (39). The Rock-Eval T_{max} of the sediments is 424 °C, which indicates that the organic matter experienced a relatively mild thermal history and has not entered the window for hydrocarbon generation (Table S6).

Both ink sacs were collected in situ and exposed by splitting the rock with a knife. Portions of the ink sacs and sediments were removed by etching the surface of the fossils with the tip of a screwdriver. These portions were then ground to a fine powder using an agar mortar. *S. officinalis* melanin, isolated from ink sacs of *S. officinalis*, was obtained from Sigma-Aldrich. DHI and DHICA were prepared as described by Wakamatsu and Ito with minor modifications (40). DHI-melanin and DHICA-melanin were prepared by tyrosinase oxidation as described in Ozeki et al. with minor modifications (25).

Scanning Electron Microscopy. SEM was used to characterize the morphology of fossil and contemporary ink. Samples (0.5 mg) were suspended in 0.500 mL of ultrapure deionized water and vortexed for 30 s. Prior to dark storage at 4 °C, 2 μL of each sample was dropped on a silicon wafer chip (5 × 5 mm) and dried in the dark under N_2. Samples were then mounted on a stainless steel peg. To increase resolutions, samples were coated with a 10-nm layer of Au/Pd by applying argon plasma for 3 min at 10 mA using a Hummer V sputter coater. Representative images were captured on an XL-SEG/SFEG SEM operated at 5–10 kV in ultrahigh-resolution mode with a spot size of 1.0 and working distance of 5.0–7.5 mm. Dimensions of the structures captured were measured using analySIS XL DOCU software. Images and dimensions of the fossil and *S. officinalis* structures are shown in Fig. 1 *C–E*.

Alkaline Hydrogen Peroxide Oxidation. To quantify the production of various pyrrole acids (PTCA, PDCA, isoPTCA, and PTeCA) from melanin samples, alkaline hydrogen peroxide degradation was performed as described in Ito et al. (17). In brief, approximately 1–4 mg of specimen was taken in a 10-mL screw-capped conical test tube, to which 100 μL water, 375 μL 1 mol/L K_2CO_3, and 25 μL 30% H_2O_2 (final concentration: 1.5%) were added. The mixture was mixed vigorously at 25 °C for 20 h. The residual H_2O_2 was decomposed by adding 50 μL 10% Na_2SO_3 and the mixture was then acidified with 140 μL of 6 mol/L HCl. The reaction mixture was centrifuged at 4,000 g for 1 min, and an aliquot (80 μL) of the supernatant was directly injected into

the HPLC system. H_2O_2 oxidation products were analyzed with the HPLC system consisting of a JASCO 880-PU liquid chromatograph (JASCO Co.), a Shiseido C_{18} column (Capcell Pak, Type MG; 4.6 × 250 mm; 5 μm particle size; Shiseido) and a JASCO UV detector monitored at 269 nm. The mobile phase was 0.1 mol/L potassium phosphate buffer (pH 2.1): methanol, 85:15 (vol/vol). Analyses were performed at 45 °C at a flow rate of 0.7 mL/min. The results for GSM 122841 and GSM 120386 are presented in Fig. 2*B* and Fig. S1*A*. The results are also tabulated, along with *S. officinalis* and the background sediments, in Table S1.

High-Resolution Liquid Chromatography–Mass Spectrometry. To confirm the identity of the degradation products PTCA, PDCA, PTeCA, and isoPTCA by mass spectrometry, we oxidized 20 mg of fossil ink sac powder (GSM 120386) in 4.0 mL of 1 mol/L K_2CO_3 with 0.5 mL 30% H_2O_2 for 20 h, extracted degradation products with ethyl acetate after decomposition of H_2O_2 and acidification to pH 1, and subjected the products to preparative HPLC using a Shiseido C_{18} column (Capcell Pak, Type MG; 20 × 250 mm plus 3.5 mm precolumn; 5 μm particle size; from Shiseido) at 25 °C and at a flow rate of 7.0 mL/min. The mobile phase was 0.4 mol/L formic acid:methanol, 80:20 (vol/vol). The pyrrole acids were individually collected as described above, and then mass spectrometry measurements of each product was performed with high-performance liquid chromatography–time of flight–mass spectrometry (LC–MS–TOF) as described below.

A 10 μL injection of each degradation product at a concentration of 60–80 μM in a 75:25 mixture of LC grade methanol and water solution was injected onto an Agilent 1200 Series high-performance liquid chromatography system (HPLC; Agilent Technologies Inc.) and separated using a Ascents Express 5 cm × 2.1 mm × 2.7 μm C_{18} column (Supelco Analytical). The HPLC was connected with a standard ESI interface to an Agilent Technologies 6224 MS–TOF to obtain high-resolution exact mass measurements.

The LC–MS–TOF was operated at a flow rate of 0.3 mL/min using a linear gradient of 0.3% formic acid, 98% water, and 2% acetonitrile (A) and 0.3% formic acid, 98% acetonitrile, and 2% water (B) as the mobile phase. The gradient program started with 0% B at 0 min and increased to 55% B during the 13 min program. The MS used an electrospray ionization (ESI) source in the negative mode. The desolvation temperature was set to 300 °C using nitrogen as the desolvation gas at 11 L/min at a nebulizer pressure of 227.5 kPa.

Total ion chromatographs and the associated MS spectrum are shown for the isolated PTCA, PDCA, isoPTCA, and PTeCA from GSM 120386 are shown in Fig. S2 *A–D*, respectively. The quantitative MS data for the parent ion for each degradation product are given in Table S2. These data confirm unambiguously that the degradation products from the fossil melanins are the pyrrole acids characteristic of melanins.

Standards of PTCA and PDCA were prepared as described in Ito and Wakamatsu with minor modifications (20). Standard of PTeCA was prepared as described in Ward et al. (24). Standard of isoPTCA was prepared by a chemically straightforward method by the small molecules facility at Duke University.

Electron Paramagnetic Resonance Spectroscopy. Eumelanin exhibits a characteristic asymmetric, 4–6 G wide single-line EPR spectra with a g value of approximately 2.004 at X-band (approximately 9.5 GHz) (14). We used a Varian Centuryline E-109 X-band EPR spectrometer interfaced with a PC using a Platform-Independent Data Acquisition Module model 401–012 made by Scientific Software Services (EWWIN 4.21) with frequency measured using an EIP Autohet frequency counter (Model 351D) to acquire the EPR spectra for fossil melanin, fossil sediment, and modern melanin samples. The EPR spectra for fossil melanins (Fig. 2*C* and Fig. S1*B*) are identical to that of *S. officinalis* melanin, and characteristic of the free radical signal associated with melanins. The line widths and g-factors for GSM 122841 and GSM 120386 are, respectively, 5.6 G and 5.7 G and 2.0028 and 2.0026. The concentration of melanin preserved in the two samples is not known, and so the relative intensity of the fossil EPR spectra does not provide information about the relative free radical concentrations. The background sediment, however, was analyzed on the same quantity of sample and plotted on the same scale as the fossil melanin to provide a qualitative comparison of the melanin present in the pigment and sediment of each sample.

Optical Absorption. Optical absorption spectra of melanin are broad and monotonic. The absorbance of fossilized melanin, sediments, and *S. officinalis* melanin, taken at 500 nm, are compared in Table S1. To prepare the solutions, 0.1 to 5 mg of each specimen was placed in a 10-mL screw-capped conical test tube and 100 μL water and 900 μL Soluene-350 (Perkin-Elmer) were added. The tubes were vortex-mixed and heated at 100 °C (boiling water bath) for 15 min. This was subsequently repeated. The mixtures were then centrifuged at 4,000 g for 3 min, and the absorption spectrum of each supernatant was analyzed. The fossil melanins, fossil sediments, and *S. officinalis* melanin all exhibit absorbance at 500 nm. The absorbance at 500 nm (A_{500}) provides an estimate of the total amount of melanin in a sample (25).

Pyrolysis in Combination with Gas Chromatography–Mass Spectrometry. Py–GC–MS serves as a powerful technique for the chemical characterization of melanin without any pretreatment of the sample (27). Flash pyrolysis was conducted at 600 °C for 20 s using a Chemical Data Systems (CDS) analytical Pyroprobe 5150. The pyrolysis chamber was held at 300 °C. GC–MS analysis of the pyrolysis products was performed using an Agilent 6890 N GC coupled to a Micromass AutoSpec Ultima magnetic sector mass spectrometer. The GC oven was held at an initial 40 °C for 2 min, increased to 310 °C at a rate of 6 °C/min, and held isothermal for 20 min. Separation was achieved using a 60 m × 0.25 mm i.d. × 0.25 μm DB5–MS capillary column with helium as the carrier gas. Full scan acquisitions were performed over the range m/z 50–600 at approximately 1 scan/s. Mass spectral conditions were 70 eV ionization energy, 250 °C source temperature, and 300 °C transfer line temperature.

The distribution of major pyrolysis products of the ink sac of the Jurassic cephalopod GSM 120386 is similar to that of the modern cuttlefish *S. officinalis* (Fig. S3). The major pyrolysis products of melanin standard, including pyridine, pyrrole, benzene, phenol, indole, their alkylated homologs, 2-phenylacetonitrile and 3-phenylpropanenitrile, are present in GSM 120386. Thiophene and its alkylated derivatives, which are abundantly present in the pyrolysates of the fossil ink sac sample, are absent or occur below detection limit in the pyrolysates of modern ink sac of *S. officinalis*.

Elemental Analysis. The elemental analysis—C, H, and N—of the fossil melanin, fossil sediment, background standards for hydroxyapatite and calcium carbonate, and modern melanin specimens was performed at the Center for Organic Elemental Microanalysis at Kyoto University using combustion. From these data, the C, H and N ratio of the fossil melanin and organic content of the sediment could be determined (41). The results are given in Table S4.

Fourier Transform Infrared Spectroscopy. In preparation for IR, a portion of each sample—fossil and modern—was compressed into a KBr pellet. IR absorption spectra of the pellet were measured using a Fourier transform infrared (IR) spectrometer attached to a microscope (Nicolet 6700/Nicolet Continum; Thermo Scientific Inc.). IR spectra were measured in the wavenumber region from 700 cm^{-1} to 4,000 cm^{-1} with resolution of 4 cm^{-1}. The viewing area was 100 × 100 μm. Fig. 3*A* shows the IR absorption spectra of GSM 122841, GSM 122841 sediment, *S. officinalis* melanin, hydroxyapatite, and calcium carbonate. The spectra for GSM 120386 are shown in Fig. S1*C*.

X-ray Photoelectron Spectroscopy. The surface composition (top 5–10 nm) of fossil sediment, fossil melanin, and contemporary melanin specimens were analyzed and compared using an X-ray photoelectron spectrometer from Kratos Analytical Axis Ultra. A circle of each sample (approximately 1 cm diameter) was coated onto copper tape using a plastic spatula. A survey scan of all of the elements available on the surface except for hydrogen (Fig. 3*B* shows the survey scan for the GSM 122841 sample) and a high-resolution spectra of the 1 s orbitals of C was obtained at two points on each sample. The relative amounts of C, N, and O were determined using the peak areas and the relative sensitivity factors of the instrumentation to C, N, and O species. The binding energy charge was corrected by setting the peak corresponding to C bound only to H to 285 eV. The resulting spectra were analyzed using CasaXPS. The deconvolution of the high-resolution scan of the C peak for the GSM 122841 sample and sediment are shown in Fig. 4 *A* and *C*. The percentages of different functional groups bound to carbon, determined by fitting the high-resolution 1 s spectra of C with mixed Gaussian (30%)-Lorentzian peaks, is presented for the fossil and *S. officinalis* melanin in Table S5.

^{13}C Cross-Polarization Magic Angle Spinning Solid-State NMR. ^{13}CP-MAS SSNMR spectra were acquired on a 600 MHz spectrometer available at the NHMFL AMRIS facility at the University of Florida at Gainesville. Spectra were acquired at a spin rate of 10 kHz using a CP contact time of 2.5 ms and a recycle delay of 0.5 s. Three characteristic spectral regions were identified as follows: 10–90 ppm, aliphatic carbons, most likely due to proteinaceous material; 90–160 ppm, aromatic carbons, including indole or pyrrole type carbons within the polymer; and 160–225 ppm, carbonyl carbon atoms from amides, carboxylates, and quinones which may be associated with the melanin polymer as well as the proteinaceous material. We also ran CP contact time experiments where contact time was shortened to 0.05 ms to further differentiate protonated aliphatic carbon atoms at 90–130 ppm from non-

protonated aliphatic carbon atoms at 130–160 ppm. The spectrum for the GSM 122841 sample is shown in Fig. 4*B*; that for GSM 120386 is shown in Fig. S1*D*. The sediment spectra for GSM 122841 and GSM 120386, shown in Fig. 4*D* and Fig. S1*E*, lack the aromatic carbon and carbonyl carbon peaks found in melanin.

Rock-Eval Pyrolysis. Pyrolysis experiments were conducted using a Rock-Eval-6 standard pyrolyzer manufactured Vinci Technologies. GSM 122841 and GSM 120386 were first pyrolyzed under inert N_2 atmosphere and the residual carbon was subsequently burned in an oxidation oven. A flame ionization detector (FID) was used to detect the amount of hydrocarbons released during pyrolysis, while online infrared detectors continuously measured the released CO and CO_2. The samples were first pyrolyzed from 300 to 650 °C at a rate of 25 °C/ min. The oxidation phase starts with an isothermal stage at 300 °C, followed by an increase to 850 °C at a rate of 25 °C/ min to oxidize all of the residual carbon. The results are listed in Table S6.

ACKNOWLEDGMENTS. Fossil samples were provided by the British Geological Survey and Mr. Paddy Howe. We thank Dr. Paul Angiolillo and Jeff Rawson for their assistance with the EPR and Dr. Dubay for his assistance with the LC–MS–TOF. Dr. Dubay was supported by NSF Grant 0923097 for the project MRI: Acquisition of an MS–TOF. We also thank Dr. David Gooden and Dr. Amanda Hoertz for preparing and analyzing our degradation standards, respectively. A portion of this work was performed in the AMRIS NHMFL, a national facility operated by the University of Florida at Gainesville on behalf of the US Department of Energy and the State of Florida, which is supported by NSF Cooperative Agreement No. DMR-0654118. Research in the Summons lab was supported by a grant from the NASA Astrobiology Institute to the MIT Team. S.I. and K.W. were supported by two grants from the Japan Society for the Promotion of Science (JSPS), Nos. 20591357 and 23591659. The Briggs Lab was supported by NSF grant EAR-0720062. P.R.W. was supported by the Curry Fund, Geologists' Association. Data reported in this paper are tabulated within the *Supporting Information*.

1. Schweitzer MH (2011) Soft tissue preservation in terrestrial mesozoic vertebrates. *Annu Rev Earth Planet Sci* 39:187–216.
2. Briggs DEG, Evershed RP, Lockheart MJ (2000) The biomolecular paleontology of continental fossils. *Paleobiology* 26:169–193.
3. Ito S (1993) High-performance liquid-chromatography (HPLC) analysis of eu- and pheomelanin in melanogenesis control. *J Invest Dermatol* 100:S166–S171.
4. Simon JD, Peles DN (2010) The red and the black. *Acc Chem Res* 43:1452–1460.
5. Dadachova E, et al. (2008) The radioprotective properties of fungal melanin are a function of its chemical composition, stable radical presence and spatial arrangement. *Pigment Cell Melanoma Res* 21:192–199.
6. Zhang F, et al. (2010) Fossilized melanosomes and the color of Cretaceous dinosaurs and birds. *Nature* 463:1075–1078.
7. Vinther J, Briggs DEG, Prum RO, Saranathan V (2008) The color of fossil feathers. *Biol Lett* 4:522–525.
8. Wogelius RA, et al. (2011) Trace metals as biomarkers for eumelanin pigment in the fossil record. *Science* 333:1622–1626.
9. Li Q, et al. (2010) Plumage color patterns of an extinct dinosaur. *Science* 327:1369–1372.
10. Vinther J, Briggs DEG, Clarke J, Mayr G, Prum RO (2009) Structural coloration in a fossil feather. *Biol Lett* 6:128–131.
11. Wilby PR, Hudson JD, Clements RG, Hollingworth NTJ (2004) Taphonomy and origin of an accumulate of soft-bodied cephalopods in the Oxford Clay Formation (Jurassic, England). *Palaeontology* 47:1159–1180.
12. Liu Y, Simon JD (2003) The effect of preparation procedures on the morphology of melanin from the ink sac of *Sepia officinalis*. *Pigment Cell Res* 16:72–80.
13. Davis PG, Briggs DEG (1995) Fossilization of feathers. *Geology* 23:783–786.
14. Meredith P, Sarna T (2006) The physical and chemical properties of eumelanin. *Pigment Cell Res* 19:572–594.
15. Briggs DEG (1999) Molecular taphonomy of animal and plant cuticles: Selective preservation and diagenesis. *Philos T Roy Soc B* 354:7–16.
16. Wakamatsu K, Ohtara K, Ito S (2009) Chemical analysis of late stages of pheomelanogenesis: Conversion of dihydrobenzothiazine to a benzothiazole structure. *Pigment Cell Melanoma Res* 22:474–486.
17. Ito S, et al. (2011) Usefulness of alkaline hydrogen peroxide oxidation to analyze eumelanin and pheomelanin in various tissue samples: Application to chemical analysis of human hair melanins. *Pigment Cell Melanoma Res* 24:605–613.
18. Sealy RC, Hyde JS, Felix CC, Menon IA, Prota G (1982) Eumelanin and pheomelanins—characterization by electron-spin resonance spectroscopy. *Science* 217:545–547.
19. Sarna T, Hyde JS, Swartz HM (1976) Ion-exchange in melanin-electron-spin resonance study with lanthanide probes. *Science* 192:1132–1134.
20. Ito S, Wakamatsu K (1998) Chemical degradation of melanins: Application to identification of dopamine-melanin. *Pigment Cell Res* 11:120–126.
21. Pezzella A, d'Ischia M, Napolitano A, Palumbo A, Prota G (1997) An integrated approach to the structure of Sepia melanin. Evidence for a high proportion of degraded 5,6-dihydroxyindole-2-carboxylic acid units in the pigment backbone. *Tetrahedron* 53:8281–8286.
22. Simon JD, Peles D, Wakamatsu K, Ito S (2009) Current challenges in understanding melanogenesis: Bridging chemistry, biological control, morphology, and function. *Pigment Cell Melanoma Res* 22:563–579.
23. Palumbo A (2003) Melanogenesis in the ink gland of *Sepia officinalis*. *Pigment Cell Res* 16:517–522.
24. Ward WC, et al. (2008) Quantification of naturally occurring pyrrole acids in melanosomes. *Photochem Photobiol* 84:700–705.
25. Ozeki H, Ito S, Wakamatsu K, Thody AJ (1996) Spectrophotometric characterization of eumelanin and pheomelanin in hair. *Pigment Cell Res* 9:265–270.
26. Damste JSS, Leeuw JW (1990) Analysis, structure and geochemical significance of organically-bound sulfur in the geosphere-state-of-the-art and future-research. *Org Geochem* 16:1077–1101.
27. Stepien K, Dzierzega-Lecznar A, Kurkiewicz S, Tam I (2009) Melanin from epidermal human melanocytes: Study by pyrolytic GC/MS. *J Am Soc Mass Spectrom* 20:464–468.
28. Centeno SA, Shamir J (2008) Surface enhanced Raman scattering (SERS) and FTIR characterization of the sepia melanin pigment used in works of art. *J Mol Struct* 873:149–159.
29. Hong L, Simon JD (2006) Insight into the binding of divalent cations to sepia eumelanin from IR absorption spectroscopy. *Photochem Photobiol* 82:1265–1269.
30. Bardani L, Bridelli MG, Carbucicchio M, Crippa PR (1982) Comparative mossbauer and infrared-analysis of iron containing melanins. *Biochim Biophys Acta* 716:8–15.
31. Clark MB, Gardella JA, Schultz TM, Patil DG, Salvati L (1990) Solid-state analysis of eumelanin biopolymers by electron-spectroscopy for chemical-analysis. *Anal Chem* 62:949–956.
32. Ni M, Ratner BD (2008) Differentiating calcium carbonate polymorphs by surface analysis techniques—an XPS and TOF-SIMS study. *Surf Interface Anal* 40:1356–1361.
33. Adhyaru BB, Akhmedov NG, Katritzky AR, Bowers CR (2003) Solid-state cross-polarization magic angle spinning C-13 and N-15 NMR characterization of Sepia melanin, Sepia melanin free acid and human hair melanin in comparison with several model compounds. *Magn Reson Chem* 41:466–474.
34. Cox BM, Hudson JD, Martill DM (1992) Lithostratigraphic nomenclature of the Oxford Clay (Jurassic). *Proc Geol Assoc* 103:343–345.
35. Kenig F, Hayes JM, Popp BN, Summons RE (1994) Isotopic biogeochemistry of the Oxford Clay Formation (Jurassic), UK. *J Geol Soc (London)* 151:139–152.
36. Hudson JD, Martill DM (1994) The Peterborough Member (Callovian, middle Jurassic) of the Oxford Clay Formation at Peterborough, UK. *J Geol Soc (London)* 151:113–124.
37. Penn IE, Cox BM, Gallois RW (1986) Towards precision in stratigraphy—geophysical log correlation of upper Jurassic (including Callovian) strata of the eastern England shelf. *J Geol Soc (London)* 143:381–410.
38. Lang WD (1924) The Blue Lias of the Devon and Dorset coasts. *Proc Geol Assoc* 35:169–185.
39. Deconinck JF, et al. (2003) Environmental controls on clay mineralogy of an early Jurassic mudrock (Blue Lias Formation, southern England). *Int J Earth Sci* 92:255–266.
40. Wakamatsu K, Ito S (1988) Preparation of eumelain-related metabolites 5,6-dihydroxyindole, 5,6 di-hydroxyindole-2-carboxylic acid, and their o-methyl derivatives. *Anal Biochem* 170:335–340.
41. Liu Y, et al. (2005) Comparison of structural and chemical properties of black and red human hair melanosomes. *Photochem Photobiol* 81(1):135–144.